MICROSTRUCTURAL CHARACTERIZATION OF TiO_2–II IN THE CHICXULUB PEAK RING.
Martin Schmieder[1,2], Timmons M. Erickson[3], David A. Kring[1,2] and the IODP–ICDP Expedition 364 Science Party, [1]Lunar and Planetary Institute – USRA, Houston, TX 77058 USA (schmieder@lpi.usra.edu), [2]NASA–SSERVI, [3]Jacobs–JETS, NASA–JSC, Houston, TX 77058 USA.

Introduction: The peak ring of the ~180 km-diameter Chicxulub impact crater on the Yucatán Peninsula, Mexico, was recently drilled during IODP–ICDP Expedition 364, producing core M0077A [1]. The new core provides insights into the anatomy, composition, tectonic deformation, shock metamorphism, and post-impact overprint of crater-filling impactites and crystalline basement rocks [2]. The basement rocks were shocked to ~12.5–17.5 GPa [3], uplifted, and hydrothermally altered [4]. This study presents a combined Raman spectroscopic and electron backscatter diffraction (EBSD) study of TiO_2–II, a high-pressure polymorph of TiO_2 with an α-PbO_2 structure (orthorhombic; space group *Pbcn*; density 4.34 g/cm^3 [5,6]), in shocked granitoid rock of the Chicxulub peak ring.

Sample and Analytical Methods: We selected shocked granitoid sample 174-2 (core depth 949 m below seafloor [1,2,7]) from the Chicxulub peak ring for high-resolution analyses. The granitoid rock contains mm-sized aggregates of TiO_2 crystals replacing altered euhedral titanite. The sample was analyzed using a Leica DMLP optical microscope; a 7600f JEOL field emission gun scanning electron microscope (FEG-SEM); a CAMECA SX 100 electron microprobe; a Jobin–Yvon Horiba LabRAM HR 800 µ-Raman spectrometer (514 nm Ar laser; ~1 µm spot diameter); and an Oxford Instruments Symmetry EBSD detector on the JEOL FEG-SEM (20 kV, 16 nA, 100 nm step size for phase and orientation mapping).

Results: Individual TiO_2 crystals in sample 174-2 are up to ~70 µm in length and appear brown-translucent under the optical microscope. The TiO_2 grains commonly occur as euhedral to subhedral crystals. Micro-Raman analysis of TiO_2 crystals produced spectra with distinct bands at *ca*. 149, 173, 287, 315, 340, 356, and 532 wavenumbers (cm^{-1}) [7], in close agreement with Raman spectra for the high-pressure polymorph TiO_2–II [5,8] (Fig. 1). Some spectra reveal additional bands at 442 and 610 cm^{-1}, indicating the presence of rutile. No Raman peaks typical of anatase or brookite were obtained in sample 174-2. Backscattered-electron (BSE) imaging reveals lamellar and locally granular microtextures, as well as subparallel and intersecting sets of fractures within individual TiO_2 crystals (Fig. 2). Electron microprobe results show the TiO_2 crystals contain ≤2.5 wt% Fe_2O_3, ≤1.5 wt% Nb_2O_3, ≤0.4 wt% SiO_2, and ≤0.3 wt% Ta_2O_5.

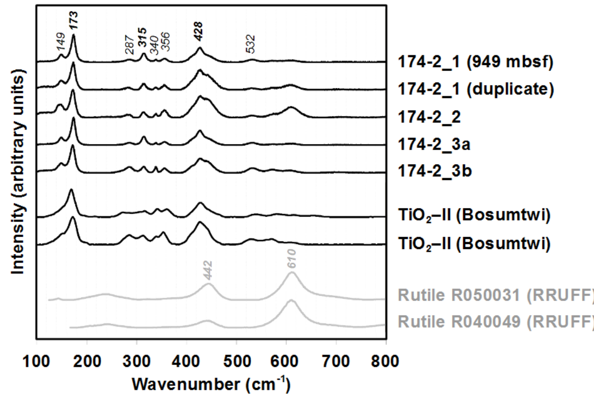

Fig. 1: Raman spectra for TiO_2–II in granitoid rock of the Chicxulub peak ring (sample 174-2), TiO_2–II from the Bosumtwi impact crater, Ghana [8], and reference spectra for rutile (RRUFF database [20]). Reference spectra for anatase and brookite are not shown. The position of laser spots in the Chicxulub sample is indicated in Fig. 2.

High-resolution EBSD mapping of individual TiO_2 crystals (Fig. 2), calibrated for rutile, anatase, brookite, and TiO_2–II (i.e., orthorhombic TiO_2 of Laue group *mmm* [9]), show a complex arrangement of locally cross-cutting lamellar and granular subdomains within each crystal investigated. EBSD phase maps reveal that the grains are composed of different TiO_2 polymorphs: (1) TiO_2–II, which forms larger, coherent, and commonly elongated lamellar domains that make up ~30 to 90% of the crystals; (2) rutile, in the form of microcrystalline granules and lamellae that locally occur between coarser-crystalline TiO_2–II; and (3) minor anatase not detected in Raman spectra, found along the margins of the TiO_2 crystals and within the surrounding matrix. The TiO_2–II correlates with slightly brighter domains in high-contrast BSE images (Fig. 2). Internal cross-cutting relationships suggest the microcrystalline-granular rutile overprints shock-produced TiO_2–II. EBSD orientation maps and pole figures show that individual TiO_2–II lamellae are related to one another by rational twin orientations, which likely formed by transformation twinning. Interphase misorientations between shock-produced TiO_2–II and neocrystalline rutile granules are systematically aligned, indicating that the solid-state reversion to rutile is crystallographically controlled.

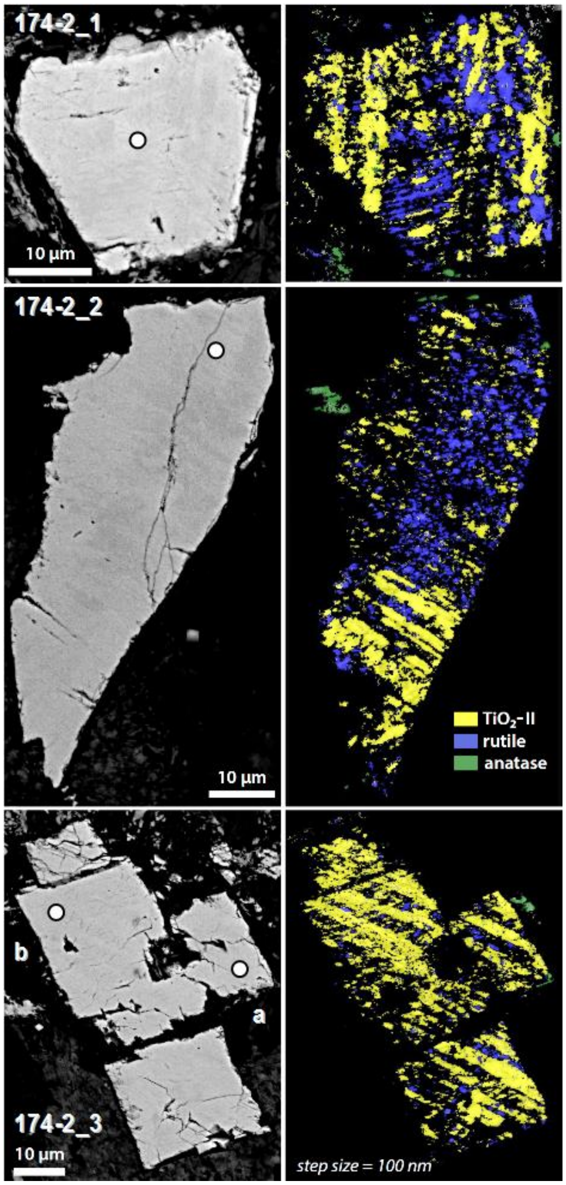

Fig. 2: Backscattered electron images (left) and corresponding EBSD phase maps (right) of TiO_2 crystals in Chicxulub peak-ring sample 174-2. White spots and labels indicate positions where Raman spectra (see Fig. 1) were collected.

Discussion and Conclusions: The discovery of TiO_2–II in rocks from the Chicxulub crater is the latest addition to a short list of terrestrial impact structures and distal ejecta layers where this shock-produced high-pressure polymorph is found [5,8,10-13]. Notably, peak-ring sample 174-2 hosts an outstanding natural occurrence of TiO_2–II, both in terms of crystal abundance and the size of individual crystals. The TiO_2–II in this and other Expedition 364 core samples [1,2,7] is the product of a long and complex pre-, syn-, and post-impact history recorded in Chicxulub's peak-ring lithologies. Based on our petrologic and microstructural observations of TiO_2 grains, we propose the following sequence of geologic events: (1) Around 340 Ma, granitoid plutons crystallized in the Maya Block [14], as indicated by U–Pb ages for magmatic titanite [7]. (2) Between ~340 Ma and 66 Ma, titanite in the granitoid rock was altered to rutile and/or anatase (+calcite, +quartz), likely during a pre-impact regional magmatic and/or hydrothermal event, and presumably under high CO_2 activity [15]. (3) During the 66 Ma Chicxulub impact, rutile and/or anatase partially to fully transformed to the high-pressure polymorph TiO_2–II at shock pressures ~12.5–17.5 GPa [3] (consistent with experimental transformation pressure constraints of ~13–20 GPa [16,17]). The shock-induced transformation to TiO_2–II may have been facilitated by pre-impact heating of the peak-ring lithologies at ~8–10 km depth [1] to ~200–250 °C (at a typical geothermal gradient of ~25 °C/km); shock metamorphic overprint of the granitoid rock contributed some additional ~100–150 °C [18]. Finally, (4) the newly formed Chicxulub crater, including shocked and uplifted rocks in its peak ring, hosted a long-lived post-impact hydrothermal system [4,19]. As the peak ring cooled, TiO_2–II incompletely back-transformed to neoblastic granules of rutile (Fig. 2).

TiO_2–II is stable below 340 °C, but rapidly (within minutes to weeks) reverts to rutile at >440–500 °C [13,16]. The formation and preservation of TiO_2–II in the Chicxulub peak ring, thus, place new petrologic constraints on shock conditions and post-impact temperatures inside the peak ring during crater cooling. Chicxulub's peak-ring lithologies must have cooled below 340°C relatively quickly (or did not significantly exceed those temperatures in the first place), so as to preserve much of the shock-produced TiO_2–II. Furthermore, these results suggest that TiO_2–II may be a common shock indicator at terrestrial impact structures, including those that experienced vigorous and long-lived post-impact hydrothermal alteration.

References: [1] Morgan J. V. et al. (2016) *Science, 354*, 878–882. [2] Gulick S. P. S. et al. (2017) Exp. 364 Prelim. Rep., IODP, 38 pp. [3] Rae A. S. P. et al. (2017) *LPS XLVIII*, abstr. #1934. [4] Kring D. A. et al. (2017) *LPS XLVIII*, abstr. #1212. [5] El Goresy A. et al. (2001) *EPSL*, *192*, 485–495. [6] Shen P. et al. (2001) *Int. Geol. Rev.*, *43*, 366–378. [7] Schmieder M. et al. (2017) 80th MetSoc, abstr. #6134. [8] McHone F. et al. (2008) *LPS XXXIX*, abstr. #2450. [9] Grey I. et al. (1988) *Mat. Sci. Bull.*, *23*, 743–753. [10] Chen M. et al. (2013) *Chinese Sci. Bull.*, *58*, 4655–4662. [11] Jackson, J. C. et al. (2006) *Am. Mineral.*, *91*, 604–608. [12] Glass B. P. and Fries M. (2008) *MAPS*, *43*, 1487–1496. [13] Smith F. C. et al. (2016) *Geology*, *44*, 775–778. [14] Kring D.A. (2005) *Chem. d. Erde*, *65*, 1–46. [15] Broska I. et al. (2007) *Lithos*, *95*, 58–71. [16] Linde R. K. and DeCarli P. S. (1969) *J. Chem. Phys.*, *50*, 319–325. [17] Syono Y. et al. (1987) in *High-Pressure Research in Mineral Physics*, pp. 385–392. [18] Stöffler D. (1984) *J. Non-Cryst. Solids*, *67*, 465–502. [19] Abramov O. and Kring D. A. (2007) *MAPS*, *42*, 93–112. [20] http://rruff.info, online.